Human Molecular Genetics, 2008, Vol. 17, No. 13 ***1956–1967***
doi:10.1093/hmg/ddn093
Advance Access published on April 1, 2008

Genetic interaction between Bardet-Biedl syndrome genes and implications for limb patterning

Marwan K. Tayeh[1,2], Hsan-Jan Yen[1,2], John S. Beck[1], Charles C. Searby[1], Trudi A. Westfall[2], Hilary Griesbach[2], Val C. Sheffield[1,*] and Diane C. Slusarski[2]

[1]Department of Pediatrics, Howard Hughes Medical Institute and [2]Department of Biological Sciences, University of Iowa, Iowa City, IA 52242, USA

Received December 20, 2007; Revised March 6, 2008; Accepted March 18, 2008

Bardet-Biedl syndrome (BBS) is a pleiotropic, genetically heterogeneous disorder characterized by obesity, retinopathy, polydactyly, cognitive impairment, renal and cardiac anomalies, as well as hypertension and diabetes. Multiple genes are known to independently cause BBS. These genes do not appear to code for the same functional category of proteins; yet, mutation of each results in a similar phenotype. Gene knockdown of different BBS genes in zebrafish shows strikingly overlapping phenotypes including defective melanosome transport and disruption of the ciliated Kupffer's vesicle. Here, we demonstrate that individual knockdown of *bbs1* and *bbs3* results in the same prototypical phenotypes as reported previously for other BBS genes. We utilize the zebrafish system to comprehensively determine whether simultaneous pair-wise knockdown of BBS genes reveals genetic interactions between BBS genes. Using this approach, we demonstrate eight genetic interactions between a subset of BBS genes. The synergistic relationships between distinct combinations are not due to functional redundancy but indicate specific interactions within a multi-subunit BBS complex. In addition, we utilize the zebrafish model system to investigate limb development. Human polydactyly is a cardinal feature of BBS not reproduced in BBS-mouse models. We evaluated zebrafish fin bud patterning and observed altered Sonic hedgehog (*shh*) expression and subsequent changes to fin skeletal elements. The SHH fin bud phenotype was also used to confirm specific genetic interactions between BBS genes. This study reveals an *in vivo* requirement for BBS function in limb bud patterning. Our results provide important new insights into the mechanism and biological significance of BBS.

INTRODUCTION

Bardet-Biedl syndrome (BBS, OMIM 209900) is a genetically heterogeneous autosomal recessive disorder characterized by obesity, retinal degeneration, post-axial polydactyly, cognitive impairment, hypogenitalism, renal and cardiovascular anomalies and a high incidence of diabetes mellitus and hypertension (1–3). To date, 12 BBS genes have been identified (4–15). Although the precise function of the individual BBS proteins is yet to be elucidated, data support roles in cilia function and intracellular transport.

In order to gain insights into the pathophysiology of BBS, we developed BBS zebrafish models and demonstrated that knockdown of any of the seven zebrafish BBS orthologs (*bbs2*, *4*, *5*, *6*, *7*, *8* and *11*) results in similar phenotypes. These phenotypes include disruption of a ciliated vesicle called Kupffer's vesicle (KV), predisposition to organ laterality defects and delayed intracellular retrograde transport (16). Mutation of BBS1 in humans leads to the most common form of BBS. The function of BBS1 is unknown. This protein contains a beta-propeller domain, indicating that it interacts with other proteins. We have recently shown that BBS1, in conjunction with BBS2, BBS4, BBS5, BBS7, BBS8 and BBS9, is part of a stable multi-protein complex known as the BBSome (17). BBS3, an ADP-ribosylation factor (ARF)-like protein known as ARL6 (18), was identified by positional cloning and the use of computational genomics (10). ARL proteins are proposed to have a role in intracellular vesicle and membrane trafficking and in microtubule assembly (18,19). Using zebrafish, we test whether *bbs1* and *bbs3*

*To whom correspondence should be addressed at: University of Iowa, 4181 MERF, Iowa City, IA 52242, USA. Tel.: +1 3193356898; Fax: +1 3193357588; Email: val-sheffield@uiowa.edu

© *The Author 2008. Published by Oxford University Press. All rights reserved.*
For Permissions, please email: journals.permissions@oxfordjournals.org

loss-of-function recapitulates prototypical BBS knockdown phenotypes including KV defect and intracellular transport delay. We also evaluate pair-wise genetic interaction between eight zebrafish BBS genes (*bbs1–bbs8*). The zebrafish model system allows for simultaneous pair-wise knockdown of multiple combinations of BBS genes, including BBS genes that code for proteins that are part of the BBSome complex, as well as proteins that are not part of the complex. Pair-wise combinations of anti-sense oligonucleotides demonstrate eight significant synergistic interactions between specific BBS genes. Of note is a central role for *bbs1* in five of these genetic interactions. The *in vivo* genetic interactions identified in this study reveals that BBS proteins that are part of the complex can result in a synergistic genetic interaction, as can proteins that are not part of the BBSome complex.

Human polydactyly is one of the cardinal features of BBS not reproduced in BBS knockout mouse models (20–23). Given that several zebrafish BBS genes are expressed in the developing fin bud (16), we evaluated fin bud patterning in BBS morphants. We focused on the zone of polarizing activity (ZPA) owing to its critical and evolutionarily conserved role in the patterning of the tetrapod limb/fin bud. We demonstrate that individual knockdown of BBS genes in zebrafish, as well as pair-wise knockdown of BBS genes, results in the expansion of Sonic hedgehog (*shh*) expression, a molecular component of the ZPA, as well as changes to subsequent skeletal elements.

RESULTS

Zebrafish *bbs1* and *bbs3* knockdowns display BBS prototypical phenotypes

Previously, we demonstrated that individual knockdown of *bbs2*, *bbs4–bbs8* and *bbs11* (9,16) generates prototypical phenotypes in zebrafish. In order to determine whether knockdowns of *bbs1* and *bbs3* result in similar phenotypes, we used antisense morpholinos to knock down these genes. Antisense morpholino oligonucleitides (MOs) were designed to target *bbs1* located on chromosome 21 and *bbs3* located on chromosome 1 in the zebrafish genome (Wellcome Trust Sanger Institute, http://www.ensembl.org). Fluorescein-tagged MOs targeting the initiator methionine (aug-MO) or the splice site of exon2 (exon2-MO) were microinjected into embryos. The MOs were uniformly distributed at 12–14 h post-fertilization (h.p.f.) and morphant embryos did not show any gross changes in general body size and morphology compared with controls. *Bbs1* and *bbs3* morphants were next evaluated for prototypical alterations including reduction or loss of a ciliated vesicle, known as Kupffer's vesicle (KV), predisposition to laterality defects and delay in melanosome retrograde transport (9,16). The KV progenitors originate in the dorsal midline and form a ciliated vesicle in the tail-bud region during somite stages (24–30). In wild-type and control MO-injected embryos at the 10–13 somite stage, the sphere-shaped KV has an average size of 50 μm (Fig. 1A and B). KV defects (reduced size to less than one-third of normal or total KV absence) were observed in a dose-dependent manner in *bbs1* MO and *bbs3* MO-injected embryos (Fig. 1; Table 1). Consistent with the proposed function of the KV in left–right axis asymmetry (24–30), zebrafish knockdown of *bbs3* showed organ laterality defects. *Bbs3* MO-injected embryos show significant jogging alterations at 22–24 h.p.f. (reversed or no jog) and looping defects at 36 h.p.f. (31), whereas low-dose *bbs3* MO or control MO-injected embryos do not show significant KV or laterality alterations (Fig. 1E; Table 1).

We previously demonstrated involvement of BBS function in general intracellular transport. Knockdown of zebrafish BBS genes (*bbs2, bbs4–bbs8* and *bbs11*) resulted in a statistically significant delay in retrograde transport (9,16). Zebrafish shuttle melanosomes within melanophores in response to visual cues and hormonal stimuli (32–35). In dark-adapted zebrafish, the melanosomes are dispersed (Fig. 1F). Melanosome aggregation (retrograde transport) is stimulated upon treatment with epinephrine (Fig. 1G) (16,36). Wild-type and control-injected embryos rapidly retract melanosomes (Fig. 1I; Table 1). In contrast, high-dose *bbs3* MO-injected embryos have significantly delayed melanosome retraction (Fig. 1H) ($P < 0.001$), whereas low-dose *bbs3* MO-injected embryos show a similar rate as control embryos ($P > 0.05$) (Table 1). Similar findings are observed with *bbs1* MO-injected embryos. Our data show that zebrafish *bbs1* and *bbs3* knockdowns result in prototypical phenotypes similar to other *bbs* gene knockdowns, including KV defects, predisposition to laterality defects and retrograde intracellular transport delay.

Genetic interaction between zebrafish BBS orthologs

Mutation of any of the 12 identified human BBS genes causes similar phenotypes, yet protein domain prediction analyses suggest that the BBS proteins do not belong to any one functional category (Supplementary Material, Fig. S1). It has been proposed that phenotypic heterogeneity among BBS patients may be due to genetic interactions between BBS genes (37). We therefore tested pair-wise knockdown of *bbs1–bbs8* in zebrafish to evaluate synergy between these genes *in vivo*. We first identified a subphenotypic dose for each the eight BBS MOs. A subphenotypic dose was defined as the highest MO dose that does not generate a significant phenotype when individually injected into zebrafish embryos (indicated as '−', Fig. 2A; Table 2). We next co-injected the 28 possible pair-wise combinations of subphenotypic dose *bbs1–bbs8* MOs. Interactions were considered significant (indicated as '+', Fig. 2A) if a statistically significant alteration in KV defects and an increase in melanosome retrograde transport were observed compared with treatment with a single low-dose MO. Eight of the 28 possible pair-wise injections resulted in synergistic interactions. All of these interactions involved either *bbs1* or *bbs2* as one of the components of the interaction. We identified five *bbs1* synergistic interactions (with *bbs2*, *bbs3*, *bbs4*, *bbs6* and *bbs7* MOs) and four *bbs2* synergistic interactions (with *bbs1*, *bbs3*, *bbs4* and *bbs6* MOs). *Bbs3*, *bbs4* and *bbs6* interacted with both *bbs1* and *bbs2*. *Bbs7* interacted only with *bbs1*. *Bbs5* and *bbs8* showed no genetic interactions with any other BBS gene. Of the eight synergistic combinations, the *bbs1* with *bbs7* pair-wise combination

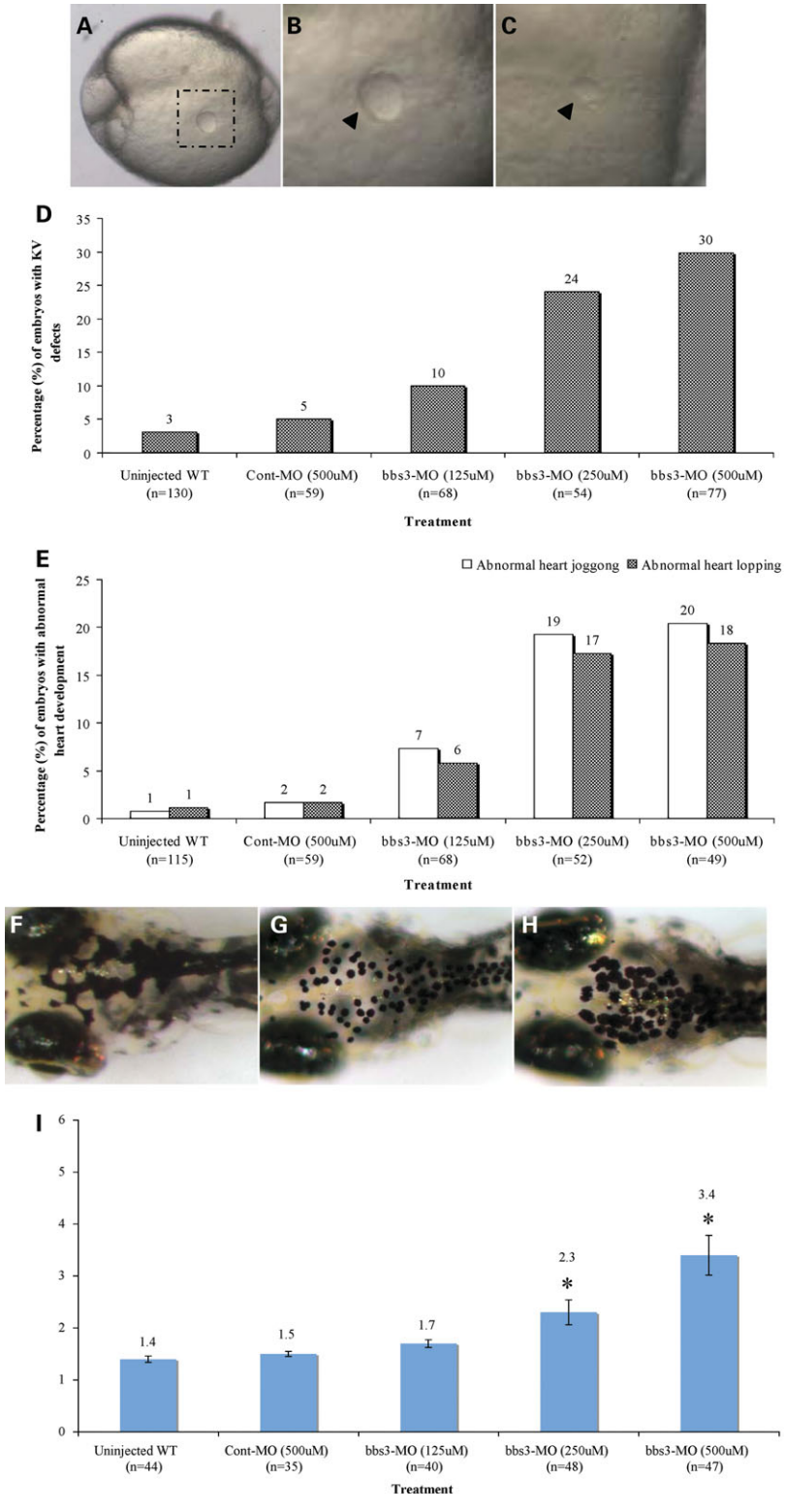

Figure 1. *bbs3* knockdown phenotypes in zebrafish. (**A**–**C**) Photographs of live zebrafish embryos at the 10–13 somite stage. (A) KV (dashed box) is a ciliated vesicle located in the tail bud region in a wild-type embryo. (B) Higher magnification of control KV (arrowhead). (C) *bbs3* MO-injected embryo with reduced KV (arrowhead). Magnification: (A) 5×; (B and C) 10×. (**D**) The percentage of zebrafish KV defects (reduced or absent) generated in MO and control sets. (**E**) Percentage of heart laterality defects observed in *bbs3* morphants and controls. (**F**–**H**) Epinephrine-induced melanosome retrograde transport, dorsal anterior view of 5-day-old larvae. (F) Wild-type larvae prior to epinephrine treatment and (G) at the endpoint of 1.5 min after epinephrine treatment. (H) *bbs3* morphant larvae showing a delayed response after 3.0 min of epinephrine treatment. (**I**) Graphical representation of epinephrine-induced melanosome retrograde transport times demonstrating a dose-dependent delay in *bbs3* knockdown when compared with wild-type and control-injected embryos. Treatment and sample size noted on the *x*-axis and percentage noted at the top of the bar. $^{*}P < 0.001$.

Table 1. *bbs1* and *bbs3* knockdown phenotypes include disruption of KV formation, heart laterality defects (jogging and looping) and a significant delay in melanosome retrograde transport

MO treatment	Percentage of KV defects	Percentage of heart jogging defects	Percentage of heart looping defects	Melanosome retrograde transport (min)
Wild-type	3 (130)	1 (115)	1 (115)	1.4 (44)
Control MO (500 μM)	5 (59)	2 (59)	2 (59)	1.5 (35)
bbs1 MO (125 μM)	9 (44)	ND	ND	1.5 (31)
bbs1 MO (250 μM)	32 (78)	22 (27)	ND	3.5* (32)
bbs3 MO (125 μM)	10 (68)	7 (68)	6 (68)	1.7 (40)
bbs3 MO (250 μM)	24 (54)	19 (52)	17 (52)	2.3* (48)
bbs3 MO (500 μM)	30 (77)	20 (49)	18 (49)	3.4* (47)

Number of embryos in each category is given in parentheses; ND, not determined.
*$P < 0.001$.

showed the most severe KV defect (Fig. 2B) and retrograde transport delay (Fig. 2C; Table 2). The other seven synergistic combinations, in order of increasing severity, are *bbs2* with *bbs4*, *bbs2* with *bbs3*, *bbs1* with *bbs2*, *bbs1* with *bbs4*, *bbs1* with *bbs6*, *bbs1* with *bbs3* and *bbs2* with *bbs6* (Table 2). To confirm synergistic interactions, we co-injected embryos with pair-wise combinations of high-dose *bbs1* MO with *bbs7* MO. We also evaluated high-dose combination of *bbs3* MO with *bbs7* MO, a non-synergistic pair. The combined high-dose *bbs1* MO with *bbs7* MO generated dramatic defects, whereas high-dose pair-wise combination of *bbs3* MO with *bbs7* MO resulted in phenotypes similar to those generated by *bbs3* MO high-dose injection alone and *bbs7* high-dose injection alone (Fig. 3A and B). The synergy data provide *in vivo* evidence for genetic interactions between specific BBS genes. These genetic interactions could indicate functional redundancy between interacting genes and/or a required stoichiometry within a complex important for the proper function of the complex.

Specificity of *bbs* knockdown

Rescue of the MO-generated phenotypes was performed to confirm the specificity of gene knockdown. We focused this component of the study on bbs1 and bbs7 for two reasons. First, the most significant genetic interaction combination was observed with *bbs1* and *bbs7*. Secondly, the bbs1 and bbs7 proteins show significant homology to each other. Co-injection of *in vitro*-transcribed *bbs1* RNA with high-dose *bbs1* MO, as well as co-injection of *bbs7* RNA with high-dose *bbs7* MO, results in rescue of both KV and retrograde transport phenotypes (Fig. 2B and C; Table 3). Thus, RNA rescue supports specificity of *bbs1* and *bbs7* MO-induced phenotypes. To investigate whether genetic interaction between BBS genes is due to functional redundancy, we co-injected high-dose *bbs7* MO with *bbs1* RNA. The high-dose *bbs7* MO-induced phenotype cannot be rescued with *bbs1* RNA. Similarly, high-dose *bbs1* MO and high-dose *bbs3* MO phenotypes cannot be rescued with *bbs7* RNA (Fig. 3A and B). These RNA rescue and pair-wise combination data provide *in vivo* evidence for specific genetic interactions between BBS genes and suggest that these genetic interactions are not due to functional redundancy. In contrast, to high-dose MO injections which lead to phenotypes, the individual low-dose MO injections of BBS MOs do not generate phenotypes, unless combined with a specific second low-dose BBS MO. Furthermore, RNA rescue of synergistic interactions was evaluated. Phenotypes generated from combined low-dose injection of *bbs1* MO with *bbs7* MO were rescued with *bbs7* RNA alone, as well as with *bbs1* RNA alone (Table 3). The ability of *bbs1* RNA or *bbs7* RNA to rescue the combined low-dose knockdown indicates that partial knockdown of either *bbs1* or *bbs7* alone does not result in complete loss of function of the BBSome complex.

Altered patterning in the zebrafish pectoral fin bud

Since polydactyly is one of the cardinal features of human BBS, we explored the possibility of fin bud patterning defects in BBS morphants. Indeed, BBS genes are broadly expressed, yet by 36 h.p.f. *bbs7* shows anterior enrichment, with notable expression in the developing fin bud (16). In BBS morphants, overall fin size was indistinguishable from wild-type, suggesting relatively normal fin growth and viability. Zebrafish pectoral fins and tetrapod forelimbs have evolved from a common ancestral appendage and share similar morphology and similar underlying molecular mechanisms (38–43), including the ZPA (44,45) which is localized at the posterior mesenchyme of the fin/limb bud (Fig. 4A). The ZPA signals positional information important for the specification of the digits. In chick limb bud, grafting an additional ZPA anterior to the original ZPA resulted in formation of extra digits resembling human polydactyly (44). Sonic hedgehog (Shh) is expressed in the posterior vertebrate limb bud mesenchyme and mediates the functions of the ZPA, in a concentration dependent manner, in both zebrafish fin buds and tetrapod limb buds (46). Since increased ZPA function or shh activity may lead to polydactyly, we evaluated *shh* expression. In wild-type embryos, s*hh* is expressed in a crescent-shaped domain in the posterior region of the pectoral fin bud (Fig. 4B). This expression domain is unchanged in control and low-dose MO-injected embryos (*bbs1*, *bbs3* and *bbs7*). The pectoral fin *shh* expression domain in high-dose *bbs1* or *bbs7* morphants demonstrates an anterior expansion, whereas *shh* expression in the dorsal midline remains unchanged (Fig. 4C). Consistent with the previously identified genetic interactions, pair-wise combination of low-dose MO of *bbs1* with *bbs7* also demonstrated expanded *shh* expression (Fig. 4D), whereas pair-wise combination of low-dose MO of *bbs3* with *bbs7* appears the same as wild-type (data not shown). The average area of *shh* expression in the pectoral fin bud was measured using the ImageJ program (47) and confirmed statistically significant ($P < 0.001$) increases in high-dose *bbs1* MO, high-dose *bbs7* MO and *bbs1* with *bbs7* low-dose combination in comparison with wild-type embryos (Fig. 4E). Thus, in the developing fin bud, we observe an increased ZPA/SHH domain without perturbing overall limb/fin growth.

A

	bbs1	bbs2	bbs3	bbs4	bbs5	bbs6	bbs7	bbs8
Cont	-	-	-	-	-	-	-	-
bbs1		+	+	+	-	+	+	-
bbs2			+	+	-	+	-	-
bbs3				-	-	-	-	-
bbs4					-	-	-	-
bbs5						-	-	-
bbs6							-	-
bbs7								-

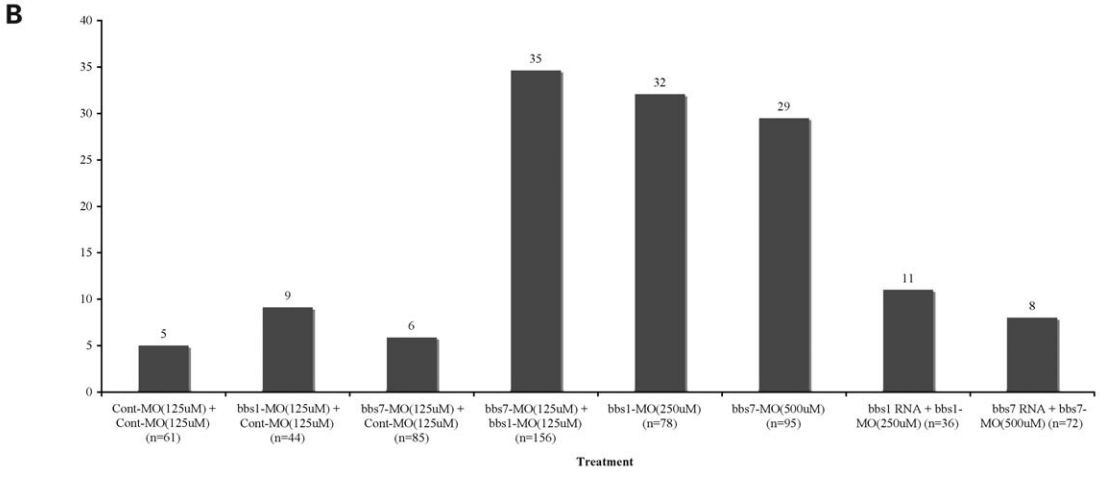

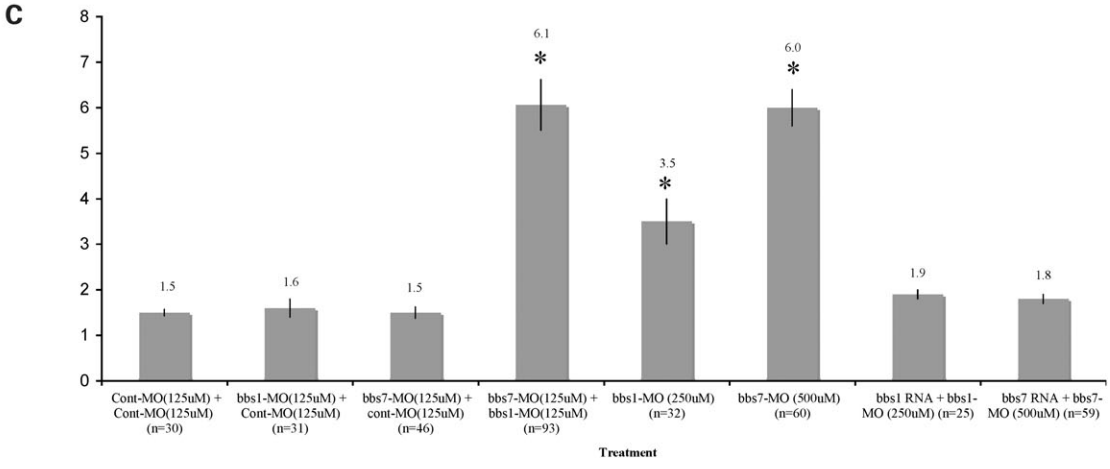

Figure 2. Genetic interaction between eight BBS genes (*bbs1–bbs8*). (**A**) Twenty-eight subphenotypic pair-wise combinations of BBS MO demonstrated only eight synergistic interactions, noted as '+' sign. Genetic interactions result in (**B**) KV disruption and (**C**) epinephrine-induced melanosome retrograde transport delay when compared with control and low-dose BBS MO-injected embryos. Specific RNA can rescue KV disruption and melanosome retrograde transport delay. Control MOs were added when necessary to maintain uniform final concentration of MO in the injection mix. $^{*}P < 0.001$; Cont, control.

Since genetic mutants for *shh* demonstrate loss or reduction of the skeletal elements of the pectoral fin (46), we next determined whether the expanded *shh*-signaling in the fin bud of BBS morphants induces expansion of pectoral fin structures. In the pectoral fin of 6–7-day-old larvae, the most proximal skeletal element is the cleithrum (Cl), which extends

Table 2. Summary of genetic interaction evaluated by BBS gene knockdown

Combined low-dose MO (*n*)	Percentage of KV defect	Melanosome retrograde transport (min)
Control + Control (61)	5	1.4
bbs1 + Control (44)	9	1.5
bbs3 + Control (68)	8	1.7
bbs7 + Control (85)	6	1.4
bbs1 + bbs7 (156)	35	6.1*
bbs2 + bbs4 (78)	30	5.0*
bbs2 + bbs3 (65)	26	5.0*
bbs1 + bbs2 (58)	24	3.8*
bbs1 + bbs4 (65)	23	3.5*
bbs1 + bbs6 (58)	23	3.0*
bbs1 + bbs3 (47)	22	2.9*
bbs2 + bbs6 (43)	21	2.5*

Subphenotypic paired combinations of MOs targeting specific BBS genes demonstrated phenotypes similar to individual BBS knockdown, including KV defect and melanosome retrograde transport delay; *n*, number of embryos.
*$P < 0.001$.

dorsoventrally (Fig. 5A). Flanking the Cl is the scapulocoracoid (Sc), which extends along the base of the fin, and the most distal element is the fin. Alcian Blue staining in wild-type identifies the rod-like Cl (Fig. 5B, arrow) and adjacent Sc (Fig. 5B, arrowhead). BBS morphant embryos demonstrate an enlarged Sc (Fig. 5C, arrowhead), where the distal posterior end of the Sc appears to have disorganized and/or extra cell layers compared with wild-type (Fig. 5B). Consistent with the genetic interaction data, *bbs1* with *bbs3* and *bbs1* with *bbs7* subphenotypic dose combinations also demonstrate thickened Sc (Fig. 5D, arrowhead), whereas *bbs3* with *bbs7*, which has no synergistic effect on KV or retrograde transport, demonstrates Sc structure similar to wild-type (data not shown). Thus, compromised BBS function by MO injection results in expanded *shh* expression and subsequently patterning changes in the skeletal elements of the pectoral fin. Although, zebrafish do not form digits, these results indicate that limb patterning defects observed in BBS patients result from SHH expression abnormalities.

DISCUSSION

Twelve genes have been shown to independently cause BBS in humans. Human BBS patients display similar features independent of the primary mutated gene. We have previously shown that individual knockdown of several zebrafish BBS genes (*bbs2, bbs4–bbs8* and *bbs11*) results in common zebrafish phenotypes including abnormal KV formation, cilia abnormalities and melanosome transport defects (9,16). In this study, we demonstrate that the individual loss-of-function of *bbs1* or *bbs3* in zebrafish results in the same phenotypes as knockdown of other zebrafish BBS genes. In addition, we have now used the zebrafish model system to identify genetic interactions between BBS genes by simultaneously knocking down pair-wise combinations of genes. For this *in vivo* analysis of genetic interactions, the 28 possible pair-wise combinations of BBS genes (*bbs1–bbs8*) were tested at doses that do not produce a phenotype when an individual morpholino is used (subphenotypic dose). At the subphenotypic doses used in this study, eight pair-wise synergistic interactions were identified. Prior to this study, no animal model for BBS polydactyly has been generated. Using the zebrafish model system, we identified altered patterning of the fin bud and subsequent changes to fin skeletal elements. Since the zebrafish fin bud is orthologous to human limb bud, this study suggests a link between post-axial polydactyly observed in BBS patients and altered *shh* expression in the developing limb/fin bud.

BBS3 function required for cilia function and intracellular vesicular transport

BBS3 (ARL6) is an ARF-like protein (10). Data support diverse functional roles for ARL proteins, including regulation of intracellular vesicle and membrane trafficking and microtubule assembly (18,19). Our loss-of-function data demonstrates that *bbs3* results in the same zebrafish phenotypes as other BBS knockdowns, including KV defects and intracellular retrograde transport delay. Cilia found in the KV appear to be initially formed in *bbs3* knockdown zebrafish, but the cilia are prematurely lost and do not function in forming a normal KV. It has recently been shown that seven BBS proteins (BBS1, 2, 4, 5, 7, 8 and 9) form a complex known as the BBSome (17). The BBSome appears to play a role in ciliogenesis, at least in part, by interacting with the Rab8 GTP/GDP exchange factor (Rabin8). Rab8GTP enters primary cilia and promotes extension of the ciliary membrane. Preventing Rab8GTP production blocks ciliation and yields characteristic BBS phenotypes in zebrafish (17). Although not a part of the BBSome, the data presented here demonstrating that bbs3 knockdown results in defects in KV and nodal cilia, as well as in melanosome (lysosome related organelles) transport, support a role for BBS3 and other BBS proteins in vesicular transport to the cilium (9,16).

Genetic interaction between BBS genes

Human BBS patients show a wide range of phenotypic variability. Variation is seen among patients even within the same family (and hence with the same primary BBS mutations), indicating genetic and/or environmental modifiers of the phenotype. The phenotypic variability and the extensive genetic heterogeneity of BBS raise the possibility of complex interactions among BBS genes (37). In this study, we identified eight genetic interactions from the total of 28 possible pair-wise genetic interactions tested. Of note, each of the eight synergistic interactions resulted in KV defects and delayed melanosome transport. No synergistic interactions were observed that affected only a subset of the phenotypes. In each case, increasing the dose of both morpholinos above the subphenotypic dose resulted in increased severity of the BBS knockdown phenotypes beyond that observed for individual high-dose knockdown, supporting the hypothesis that BBS genes can modify each other's phenotypes.

BBS complex interactions could be due to redundant roles, parallel pathway function or a stoichometric requirement within a protein complex such as the BBSome, to name a few possibilities. In this study, we demonstrated that individual high-dose MO-induced defects can be rescued by

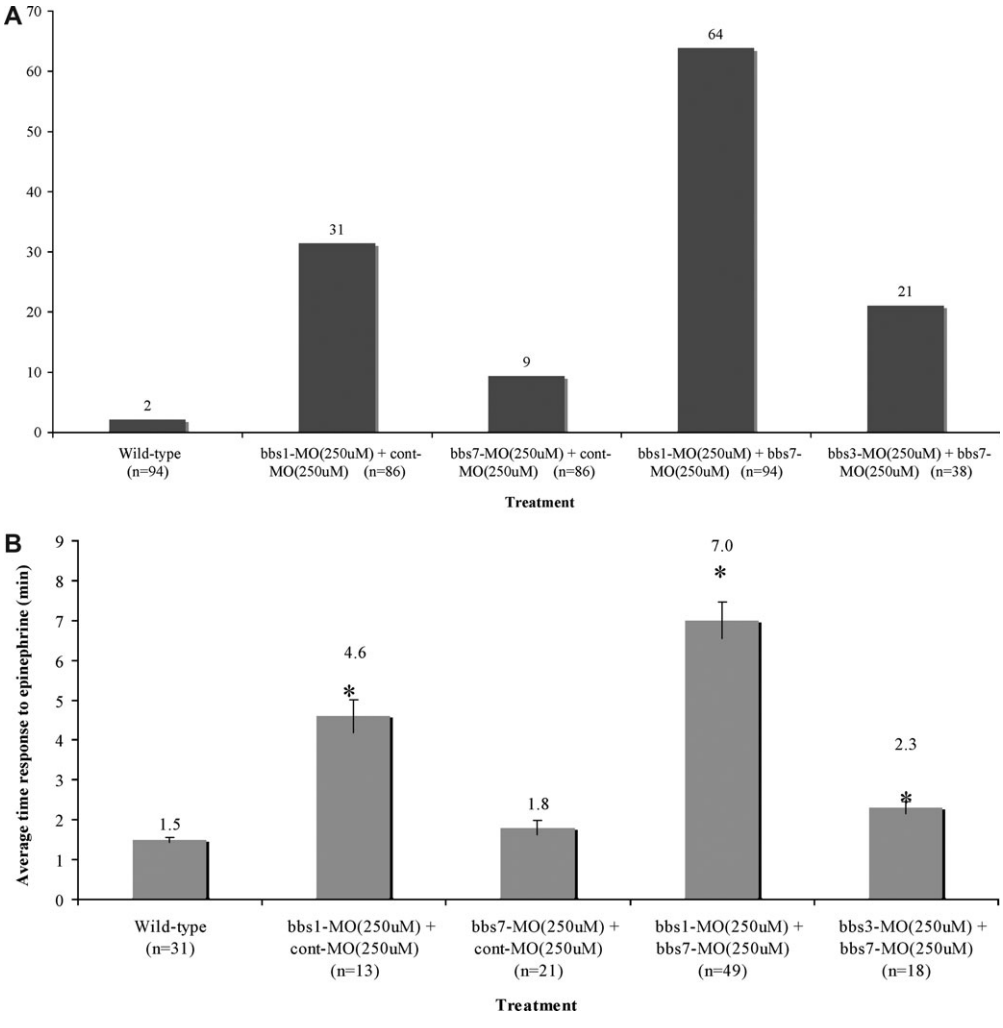

Figure 3. Medium-dose knockdown of genetically interacting BBS genes results in an increased severity and penetrance of BBS knockdown phenotypes, including (**A**) KV disruption and (**B**) epinephrine-induced melanosome retrograde transport when compared with wild-type, control injected and embryos injected with MO combinations of *bbs* genes that do not genetically interact. Treatment and numbers of embryos noted on the *x* axis and values on the top of the bars. $^{*}P < 0.001$; Cont, control.

Table 3. BBS gene knockdown rescue and test for redundant function

MO treatment (*n*)	RNA	Percentage of KV defects	Melanosome retrograde transport (min)
Control (500 μM) (302)	—	3	1.5
Control (500 μM) (41)	*bbs1*	7	1.8
Control (500 μM) (49)	*bbs7*	4	1.5
bbs1 MO (250 μM) (78)	—	32	3.5*
bbs1 MO (250 μM) (36)	*bbs1*	11	1.9
bbs7 MO (500 μM) (95)	—	29	6.0*
bbs7 MO (500 μM) (72)	*bbs7*	8	1.8
bbs1 MO (250 μM) (98)	*bbs7*	32	3.4*
bbs7 MO (500 μM) (48)	*bbs1*	27	6.1*
bbs7 MO (125 μM) + *bbs1* MO (125 μM) (51)	*bbs1*	10	1.9
bbs7 MO (125 μM)+*bbs1* MO (125 μM) (43)	*bbs7*	9	1.9
bbs3 MO (500 μM) (38)	*bbs7*	34	3.0*

BBS genes do not display functional redundancy. *bbs7* knockdown phenotypes can be rescued only by specific *bbs7* mRNA. Subphenotypic paired combination of *bbs1* with *bbs7* phenotypes can be rescued with either *bbs1* or *bbs7* mRNA. Overexpression of *bbs1* or *bbs7* mRNA has no significant phenotypes; *n*, number of embryos.
$^{*}P < 0.001$.

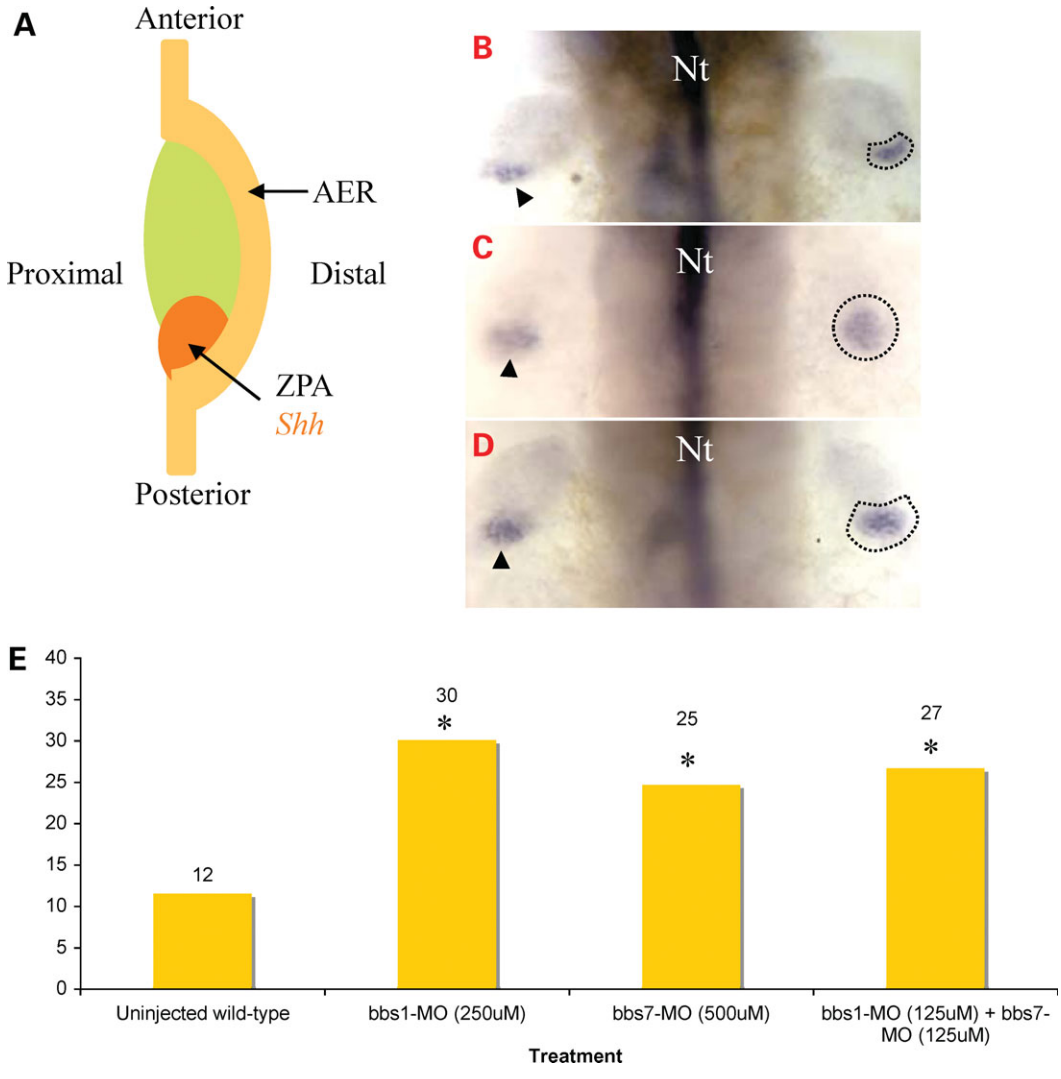

Figure 4. Zone of polarizing activity (ZPA) of the pectoral fin bud and Sonic hedgehog (SHH). (**A**) Schematic representation of zebrafish fin bud prior to 48 h.p.f. ZPA is localized posteriorly and can be labeled with *shh* expression. Whole-mount *in situ* hybridization using *shh* as a probe in the pectoral fin bud of 42 h.p.f. (**B**) wild-type, (**C**) bbs7 morphant and (**D**) low-dose *bbs1* MO with *bbs7* MO combination. Arrowhead denotes shh expression in the limb bud on one side, and the area of expression is outlined on the other side. (**E**) Graphical representation of the measured area (μm^2) of *shh* expression domain in the pectoral fin bud of BBS morphants and wild-type. $^*P < 0.001$.

co-injection of a wild-type form of the gene-specific mRNA (i.e. *bbs7* mRNA rescues the high-dose *bbs7* MO phenotype), but not by increased levels of other BBS proteins. For example, *bbs1* mRNA does not rescue high-dose *bbs7* MO-induced defects and vice versa, arguing against functional redundancy. In contrast, an individual mRNA is sufficient to rescue the subphenotypic combined knockdown MOs (i.e. *bbs7* mRNA can rescue the low-dose combined *bbs7* with *bbs1* MO-induced defects), suggesting a required stoichiometry within a complex. A recent study by Nachury *et al.* (17) has identified a BBS complex (the BBSome) and reported that components of the complex are present in stoichiometric amounts.

The identification of the BBSome complex consisting of seven of the 12 known BBS proteins (BBS1, BBS2, BBS4, BBS5, BBS7, BBS8 and BBS9) (17) can be used to categorize the known BBS proteins into those that are part of the BBSome and those that are not part of this complex (BBS3, BBS6, BBS10, BBS11 and BBS12). This information, along with the genetic interaction data from the current study, allows the determination of whether BBS pair-wise genetic interactions result from impairment of two BBSome proteins, impairment of a component of the BBSome and a non-BBSome component and/or simultaneous impairment of two non-BBSome proteins. The first two types of interactions were observed. For example, the strongest interaction was seen between two BBSome components (BBS1 and BBS7). In addition, the two non-BBSome proteins studied (BBS3 and BBS6) were each shown to genetically interact with specific components of the BBSome (BBS3 with BBS1 and BBS2; BBS6 with BBS1 and BBS2), but not with other BBSome components and not with each other. Furthermore, direct physical interactions within the BBSome complex do not predict genetic interactions. For example, BBS7 physically

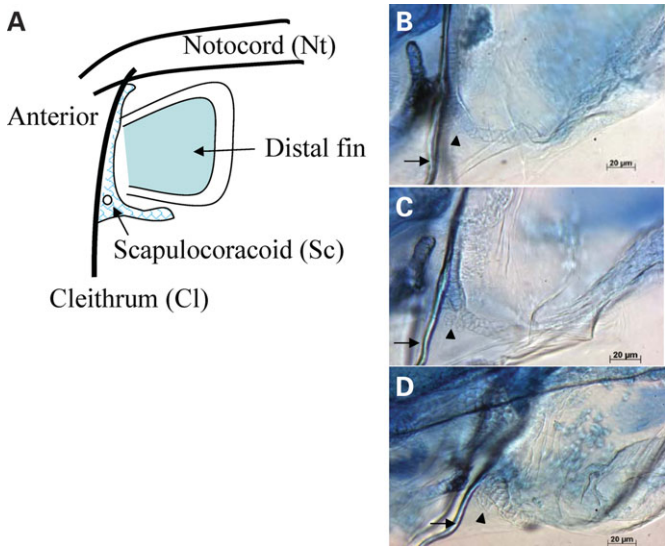

Figure 5. Zebrafish pectoral fin cartilage staining. (**A**) Schematic representation of the fin structures: Cl as a dorsoventral line (arrow); Sc distal to Cl and proximal to fin. (**B**–**D**) Alcian Blue staining of the pectoral fin shows prototypical cartilage structure in 6-day-old (B) wild-type larvae, whereas (C) *bbs7* morphant larvae and (D) low-dose combination of *bbs1* MO with *bbs7* MO show enlarged Sc structure with two to three cell lines at the proximal posterior region of Sc (arrowhead).

interacts directly with BBS2 and not with BBS1 (17). However, BBS7 genetically interacts with BBS1, but not with BBS2.

On the basis of finding of a heterozygous variant in MGC1203 in a few BBS patients, Badano *et al*. (48) utilized zebrafish to evaluate epistatic effect of *mgc1203* on BBS genes and reported that modest suppression of *mgc1203* exerts an epistatic effect on the developmental phenotype of BBS morphants. Similarly, our subphenotypic knockdowns of specific zebrafish BBS genes suggest that some BBS genes have an epistatic effect on the phenotype of other BBS genes. It is noteworthy that two independent studies utilized similar subphenotypic approach in zebrafish to evaluate genetic interactions of *bbs10* and *bbs12* genes (12,15). It should be noted that the authors reported gastrulation defects as a BBS MO-induced phenotype (12,15,48) and utilized this phenotype to identify potential interactions between BBS genes. The morphant embryos in our study do not show any gross changes in general body size and morphology. The cilia defect and transport delay phenotypes observed in the current study are biologically relevant to the human disorder.

Of clinical relevance, our data provide insight into non-Mendelian modes of BBS inheritance. Triallelic inheritance has been reported in a small subset of BBS cases (49–54). Our zebrafish data indicate that high-dose knockdown of individual BBS genes results in KV cilia and vesicle transport phenotypes (9,16). These data support mouse knockout data that complete loss of function of a single BBS protein is sufficient to induce BBS phenotypes (20–22). The genetic interaction data presented here suggest that functionally hypomorphic alleles of two specific BBS proteins could combine to result in digenic inheritance of BBS. On the basis of the zebrafish data demonstrating relevant phenotypes induced by simultaneous knockdown of two BBS genes, it is tempting to hypothesize that heterozygosity in two BBS genes (double heterozygosity) could be sufficient to manifest some BBS phenotypes. Such an occurrence has not been reported. The availability of multiple BBS mouse models will facilitate testing of this hypothesis.

A link between SSH and BBS limb defects

BBS pathophysiology has been linked to defects in cilia function and intracellular transport. Yet, polydactyly is not consistently reported in ciliary diseases (55–58). Therefore, mechanistic links between cilia function and polydactyly remain unclear. Since the zebrafish paired fins and tetrapod limbs are phylogenetically related, morphologically similar (42,43,59) and display similar gene expression patterns in the developing limb/fin buds, we can use this system to analyze the molecular mechanisms that underlie their early development (38–43). BBS loss-of-function demonstrates expanded *shh* expression in the pectoral fin bud without affecting *shh* neural tube expression. Furthermore, *shh* is required for fin/limb endoskeletal development (43), and the zebrafish *shh* mutant (*syu*) showed loss of pectoral girdle skeletal elements (46,60), while ectopic expression of chicken *Shh* in limb bud micromass culture induced novel cartilage nodules (61). Analysis of the skeletal elements in BBS knockdown larvae revealed a thickened scapulocoracoid of the pectoral fin consistent with increased *shh* expression in the pectoral fin bud. Although cilia function and IFT have been reported to play a role in SHH signaling (56,62,63), our current study uses *shh* as markers for the ZPA. In addition, *shh* expression in the midline is unperturbed. Further study is needed to directly address the role of cilia or intracellular transport in *shh* regulation in the BBS morhpants. However, our data provide *in vivo* evidence for a role of BBS function in limb/fin bud patterning resulting in increased *shh* signaling.

MATERIALS AND METHODS

MO antisense

Antisense MOs were designed and purchased from Gene Tools, LLC. MOs were microinjected in approximately 3 nanoliter volumes into one to eight cell embryos at concentrations ranging from 125 to 500 mM. Zebrafish MO sequences are *bbs1*_aug (GGGAACAGATGACATGGTTGTTTTG); *bbs1*_exon2 (TGAAACTCACCAAT GCATGAGGAGA); control MO *bbs1*_5mis (TAAGaGTGAtGATGGcCACTtGCAT); *bbs3*_aug (AGCTTGTCAAAAAG CCCCA TTTGCT); *bbs3*_exon2 (TACATCTTTTATTTTCACCTTGAGG) and control MO *bbs3*_5mis (AGgTTcTCAAAAAaCCCgATTTcCT).

Pair-wise combination of *bbs* morpholinos

Two different BBS MOs targeting *bbs1*–*bbs8* were combined at subphenotypic low doses (125 μM each) and microinjected into one to eight cell embryos. Controls for these experiments were combinations of low dose of each BBS MO and a control MO (125 μM each). The final concentration of MOs injected

into any embryo in this experiment was always constant (250 μM).

Analysis of the KV

Vesicles in embryos with a diameter less than one-third that of wild-type were considered reduced and embryos in which vesicles could not be morphologically identified were scored as absent. Live embryos were photographed with a Zeiss Axiocam on a stereoscope.

Melanosome transport assay

Day 5 larvae were exposed to epinephrine (50 mg/ml, Sigma, E4375) added to embryo medium (64) for a final concentration of 500 μg/ml. Melanosome retraction was continuously monitored under the microscope and the endpoint was scored when all melanosomes in the head and the trunk were perinuclear.

Rescue of knockdown phenotype

Morpholino-resistant BBS RNA was subcloned into pCS2+ expression vector (65). Synthetic RNA was made with mMessage mMachine (Ambion). mRNA (50 ng/μl *bbs1* and 100 ng/μl *bbs7*) was co-injected with appropriate MO.

Whole-mount *in situ* hybridization of *shh* in the pectoral fin buds

Embryos, treated with pigment inhibitor at 12 h.p.f., were cultured to 42 h.p.f. and fixed with 4% paraformaldehyde/phosphate-buffered saline (PBS). *shh* digoxigenin-UTP RNA probes (Roche) were synthesized from the linearized templates, antisense (*Spe*I, T7 RNA polymerase) and sense (*Not*I, SP6 RNA polymerase). Whole-mount *in situ* hybridization was performed as described by Yen *et al*. (16). The area of *shh* expression was measured using ImageJ 1.37v (47). Student's *t*-test assuming unequal variance was used to evaluate statistically significant differences in the average area of *shh* expression ($P < 0.001$). Embryos were photographed at 50× magnification.

Cartilage staining

Cartilage staining was performed as described in Taylor and Van Dyke (66). Briefly, larvae at 6 day post-fertilization (d.p.f.) were fixed overnight with 4% paraformaldehyde/PBS, dehydrated gradually with absolute ethanol and stained overnight with Alcian Blue (30 mg in 8:2 ethanol:glacial acetic acid). Larvae were then bleached with 1% potassium hydroxide (1 M)/3% hydrogen peroxide, cleared with 0.5% trypsine/saturated sodium tetraborate, pH 9.1, for 2 h and stored in 7:3 glycerol:(1X) PBS. Cartilage mounts were photographed at 50× magnification.

FUNDING

This research work was supported by the National Institutes of Health (EY011298 and EY017168 to V.C.S. and CA112369 to D.C.S.). V.C.S. is an investigator of the Howard Hughes Medical Institute.

SUPPLEMENTARY MATERIAL

Supplementary Material is available at HMG Online.

ACKNOWLEDGEMENTS

We thank the members of V.C.S. and D.C.S. laboratories for their insightful discussions.

Conflict of Interest statement. None declared.

REFERENCES

1. Green, J.S., Parfrey, P.S., Harnett, J.D., Farid, N.R., Cramer, B.C., Johnson, G., Heath, O., McManamon, P.J., O'Leary, E. and Pryse-Phillips, W. (1989) The cardinal manifestations of Bardet-Biedl syndrome, a form of Laurence–Moon–Biedl syndrome. *N Engl. J. Med.*, **321**, 1002–1009.
2. Harnett, J.D., Green, J.S., Cramer, B.C., Johnson, G., Chafe, L., McManamon, P., Farid, N.R., Pryse-Phillips, W. and Parfrey, P.S. (1988) The spectrum of renal disease in Laurence–Moon–Biedl syndrome. *N. Engl. J. Med.*, **319**, 615–618.
3. Elbedour, K., Zucker, N., Zalzstein, E., Barki, Y. and Carmi, R. (1994) Cardiac abnormalities in the Bardet-Biedl syndrome: echocardiographic studies of 22 patients. *Am. J. Med. Genet.*, **52**, 164–169.
4. Slavotinek, A.M., Stone, E.M., Mykytyn, K., Heckenlively, J.R., Green, J.S., Heon, E., Musarella, M.A., Parfrey, P.S., Sheffield, V.C. and Biesecker, L.G. (2000) Mutations in MKKS cause Bardet-Biedl syndrome. *Nat. Genet.*, **26**, 15–16.
5. Mykytyn, K., Braun, T., Carmi, R., Haider, N.B., Searby, C.C., Shastri, M., Beck, G., Wright, A.F., Iannaccone, A., Elbedour, K. *et al.* (2001) Identification of the gene that, when mutated, causes the human obesity syndrome BBS4. *Nat. Genet.*, **28**, 188–191.
6. Nishimura, D.Y., Searby, C.C., Carmi, R., Elbedour, K., Van Maldergem, L., Fulton, A.B., Lam, B.L., Powell, B.R., Swiderski, R.E., Bugge, K.E. *et al.* (2001) Positional cloning of a novel gene on chromosome 16q causing Bardet-Biedl syndrome (BBS2). *Hum. Mol. Genet.*, **10**, 865–874.
7. Nishimura, D.Y., Swiderski, R.E., Searby, C.C., Berg, E.M., Ferguson, A.L., Hennekam, R., Merin, S., Weleber, R.G., Biesecker, L.G., Stone, E.M. *et al.* (2005) Comparative genomics and gene expression analysis identifies BBS9, a new Bardet-Biedl syndrome gene. *Am. J. Hum. Genet.*, **77**, 1021–1033.
8. Ansley, S.J., Badano, J.L., Blacque, O.E., Hill, J., Hoskins, B.E., Leitch, C.C., Kim, J.C., Ross, A.J., Eichers, E.R., Teslovich, T.M. *et al.* (2003) Basal body dysfunction is a likely cause of pleiotropic Bardet-Biedl syndrome. *Nature*, **425**, 628–633.
9. Chiang, A.P., Beck, J.S., Yen, H.J., Tayeh, M.K., Scheetz, T.E., Swiderski, R.E., Nishimura, D.Y., Braun, T.A., Kim, K.Y., Huang, J. *et al.* (2006) Homozygosity mapping with SNP arrays identifies TRIM32, an E3 ubiquitin ligase, as a Bardet-Biedl syndrome gene (BBS11). *Proc. Natl Acad. Sci. USA*, **103**, 6287–6292.
10. Chiang, A.P., Nishimura, D., Searby, C., Elbedour, K., Carmi, R., Ferguson, A.L., Secrist, J., Braun, T., Casavant, T., Stone, E.M. *et al.* (2004) Comparative genomic analysis identifies an ADP-ribosylation factor-like gene as the cause of Bardet-Biedl syndrome (BBS3). *Am. J. Hum. Genet.*, **75**, 475–484.
11. Li, J.B., Gerdes, J.M., Haycraft, C.J., Fan, Y., Teslovich, T.M., May-Simera, H., Li, H., Blacque, O.E., Li, L., Leitch, C.C. *et al.* (2004) Comparative genomics identifies a flagellar and basal body proteome that includes the BBS5 human disease gene. *Cell*, **117**, 541–552.
12. Stoetzel, C., Laurier, V., Davis, E.E., Muller, J., Rix, S., Badano, J.L., Leitch, C.C., Salem, N., Chouery, E., Corbani, S. *et al.* (2006) BBS10 encodes a vertebrate-specific chaperonin-like protein and is a major BBS locus. *Nat. Genet.*, **38**, 521–524.
13. Badano, J.L., Ansley, S.J., Leitch, C.C., Lewis, R.A., Lupski, J.R. and Katsanis, N. (2003) Identification of a novel Bardet-Biedl syndrome

protein, BBS7, that shares structural features with BBS1 and BBS2. *Am. J. Hum. Genet.*, **72**, 650–658.
14. Katsanis, N., Beales, P.L., Woods, M.O., Lewis, R.A., Green, J.S., Parfrey, P.S., Ansley, S.J., Davidson, W.S. and Lupski, J.R. (2000) Mutations in MKKS cause obesity, retinal dystrophy and renal malformations associated with Bardet-Biedl syndrome. *Nat. Genet.*, **26**, 67–70.
15. Stoetzel, C., Muller, J., Laurier, V., Davis, E.E., Zaghloul, N.A., Vicaire, S., Jacquelin, C., Plewniak, F., Leitch, C.C., Sarda, P. *et al.* (2007) Identification of a novel BBS gene (BBS12) highlights the major role of a vertebrate-specific branch of chaperonin-related proteins in Bardet-Biedl syndrome. *Am. J. Hum. Genet.*, **80**, 1–11.
16. Yen, H.J., Tayeh, M.K., Mullins, R.F., Stone, E.M., Sheffield, V.C. and Slusarski, D.C. (2006) Bardet-Biedl syndrome genes are important in retrograde intracellular trafficking and Kupffer's vesicle cilia function. *Hum. Mol. Genet.*, **15**, 667–677.
17. Nachury, M.V., Loktev, A.V., Zhang, Q., Westlake, C.J., Peranen, J., Merdes, A., Slusarski, D.C., Scheller, R.H., Bazan, J.F., Sheffield, V.C. *et al.* (2007) A core complex of BBS proteins cooperates with the GTPase Rab8 to promote ciliary membrane biogenesis. *Cell*, **129**, 1201–1213.
18. Pasqualato, S., Renault, L. and Cherfils, J. (2002) Arf, Arl, Arp and Sar proteins: a family of GTP-binding proteins with a structural device for 'front-back' communication. *EMBO Rep.*, **3**, 1035–1041.
19. Bhamidipati, A., Lewis, S.A. and Cowan, N.J. (2000) ADP ribosylation factor-like protein 2 (Arl2) regulates the interaction of tubulin-folding cofactor D with native tubulin. *J. Cell Biol.*, **149**, 1087–1096.
20. Fath, M.A., Mullins, R.F., Searby, C., Nishimura, D.Y., Wei, J., Rahmouni, K., Davis, R.E., Tayeh, M.K., Andrews, M., Yang, B. *et al.* (2005) Mkks-null mice have a phenotype resembling Bardet-Biedl syndrome. *Hum. Mol. Genet.*, **14**, 1109–1118.
21. Mykytyn, K., Mullins, R.F., Andrews, M., Chiang, A.P., Swiderski, R.E., Yang, B., Braun, T., Casavant, T., Stone, E.M. and Sheffield, V.C. (2004) Bardet-Biedl syndrome type 4 (BBS4)-null mice implicate Bbs4 in flagella formation but not global cilia assembly. *Proc. Natl Acad. Sci USA*, **101**, 8664–8669.
22. Nishimura, D.Y., Fath, M., Mullins, R.F., Searby, C., Andrews, M., Davis, R., Andorf, J.L., Mykytyn, K., Swiderski, R.E., Yang, B. *et al.* (2004) Bbs2-null mice have neurosensory deficits, a defect in social dominance, and retinopathy associated with mislocalization of rhodopsin. *Proc. Natl Acad. Sci. USA*, **101**, 16588–16593.
23. Davis, R.E., Swiderski, R.E., Rahmouni, K., Nishimura, D.Y., Mullins, R.F., Agassandian, K., Philp, A.R., Searby, C.C., Andrews, M.P., Thompson, S. *et al.* (2007) A knockin mouse model of the Bardet Biedl syndrome 1 M390R mutation has cilia defects, ventriculomegaly, retinopathy, and obesity. *Proc. Natl Acad. Sci. USA*, **104**, 19422–19427.
24. Supp, D.M., Brueckner, M., Kuehn, M.R., Witte, D.P., Lowe, L.A., McGrath, J., Corrales, J. and Potter, S.S. (1999) Targeted deletion of the ATP binding domain of left-right dynein confirms its role in specifying development of left–right asymmetries. *Development*, **126**, 5495–5504.
25. Supp, D.M., Witte, D.P., Potter, S.S. and Brueckner, M. (1997) Mutation of an axonemal dynein affects left–right asymmetry in inversus viscerum mice. *Nature*, **389**, 963–966.
26. Essner, J.J., Amack, J.D., Nyholm, M.K., Harris, E.B. and Yost, H.J. (2005) Kupffer's vesicle is a ciliated organ of asymmetry in the zebrafish embryo that initiates left–right development of the brain, heart and gut. *Development*, **132**, 1247–1260.
27. Essner, J.J., Vogan, K.J., Wagner, M.K., Tabin, C.J., Yost, H.J. and Brueckner, M. (2002) Conserved function for embryonic nodal cilia. *Nature*, **418**, 37–38.
28. Melby, A.E., Warga, R.M. and Kimmel, C.B. (1996) Specification of cell fates at the dorsal margin of the zebrafish gastrula. *Development*, **122**, 2225–2237.
29. Cooper, M.S. and D'Amico, L.A. (1996) A cluster of noninvoluting endocytic cells at the margin of the zebrafish blastoderm marks the site of embryonic shield formation. *Dev. Biol.*, **180**, 184–198.
30. D'Amico, L.A. and Cooper, M.S. (1997) Spatially distinct domains of cell behavior in the zebrafish organizer region. *Biochem. Cell. Biol.*, **75**, 563–577.
31. Chen, C.Y. and Schwartz, R.J. (1996) Recruitment of the tinman homolog Nkx-2.5 by serum response factor activates cardiac alpha-actin gene transcription. *Mol. Cell. Biol.*, **16**, 6372–6384.
32. Skold, H.N., Aspengren, S. and Wallin, M. (2002) The cytoskeleton in fish melanophore melanosome positioning. *Microsc. Res. Tech.*, **58**, 464–469.
33. Barral, D.C. and Seabra, M.C. (2004) The melanosome as a model to study organelle motility in mammals. *Pigment Cell Res.*, **17**, 111–118.
34. Marks, M.S. and Seabra, M.C. (2001) The melanosome: membrane dynamics in black and white. *Nat. Rev. Mol. Cell Biol.*, **2**, 738–748.
35. Blott, E.J. and Griffiths, G.M. (2002) Secretory lysosomes. *Nat. Rev. Mol. Cell Biol.*, **3**, 122–131.
36. Nascimento, A.A., Roland, J.T. and Gelfand, V.I. (2003) Pigment cells: a model for the study of organelle transport. *Annu. Rev. Cell. Dev. Biol.*, **19**, 469–491.
37. Mykytyn, K. and Sheffield, V.C. (2004) Establishing a connection between cilia and Bardet-Biedl syndrome. *Trends Mol. Med.*, **10**, 106–109.
38. Krauss, S., Concordet, J.P. and Ingham, P.W. (1993) A functionally conserved homolog of the *Drosophila* segment polarity gene hh is expressed in tissues with polarizing activity in zebrafish embryos. *Cell*, **75**, 1431–1444.
39. Ekker, M., Wegner, J., Akimenko, M.A. and Westerfield, M. (1992) Coordinate embryonic expression of three zebrafish engrailed genes. *Development*, **116**, 1001–1010.
40. Akimenko, M.A. and Ekker, M. (1995) Anterior duplication of the Sonic hedgehog expression pattern in the pectoral fin buds of zebrafish treated with retinoic acid. *Dev. Biol.*, **170**, 243–247.
41. Akimenko, M.A., Johnson, S.L., Westerfield, M. and Ekker, M. (1995) Differential induction of four msx homeobox genes during fin development and regeneration in zebrafish. *Development*, **121**, 347–357.
42. Sordino, P., van der Hoeven, F. and Duboule, D. (1995) Hox gene expression in teleost fins and the origin of vertebrate digits. *Nature*, **375**, 678–681.
43. Neumann, C.J., Grandel, H., Gaffield, W., Schulte-Merker, S. and Nusslein-Volhard, C. (1999) Transient establishment of anteroposterior polarity in the zebrafish pectoral fin bud in the absence of sonic hedgehog activity. *Development*, **126**, 4817–4826.
44. Tickle, C., Summerbell, D. and Wolpert, L. (1975) Positional signalling and specification of digits in chick limb morphogenesis. *Nature*, **254**, 199–202.
45. Saunders, J.W. and Gasseling, M.T. (1968) Ectoderm-mesenchymal interactions in the origin of wing symmetry. In Fleischmajer, R. and Billingham, R.E. (eds), *Epithelial–Mesenchymal Interactions*. Williams and Wikins, Baltimore, MA.
46. Grandel, H., Draper, B.W. and Schulte-Merker, S. (2000) Dackel acts in the ectoderm of the zebrafish pectoral fin bud to maintain AER signaling. *Development*, **127**, 4169–4178.
47. Rasband, W. (2006) *ImageJ 1.37v*. National Institute of Health, USA.
48. Badano, J.L., Leitch, C.C., Ansley, S.J., May-Simera, H., Lawson, S., Lewis, R.A., Beales, P.L., Dietz, H.C., Fisher, S. and Katsanis, N. (2006) Dissection of epistasis in oligogenic Bardet-Biedl syndrome. *Nature*, **439**, 326–330.
49. Katsanis, N. (2004) The oligogenic properties of Bardet-Biedl syndrome. *Hum. Mol. Genet.*, **13**, R65–R71.
50. Katsanis, N., Ansley, S.J., Badano, J.L., Eichers, E.R., Lewis, R.A., Hoskins, B.E., Scambler, P.J., Davidson, W.S., Beales, P.L. and Lupski, J.R. (2001) Triallelic inheritance in Bardet-Biedl syndrome, a Mendelian recessive disorder. *Science*, **293**, 2256–2259.
51. Laurier, V., Stoetzel, C., Muller, J., Thibault, C., Corbani, S., Jalkh, N., Salem, N., Chouery, E., Poch, O., Licaire, S. *et al.* (2006) Pitfalls of homozygosity mapping: an extended consanguineous Bardet-Biedl syndrome family with two mutant genes (BBS2, BBS10), three mutations, but no triallelism. *Eur. J. Hum. Genet.*, **14**, 1195–1203.
52. Badano, J.L., Kim, J.C., Hoskins, B.E., Lewis, R.A., Ansley, S.J., Cutler, D.J., Castellan, C., Beales, P.L., Leroux, M.R. and Katsanis, N. (2003) Heterozygous mutations in BBS1, BBS2 and BBS6 have a potential epistatic effect on Bardet-Biedl patients with two mutations at a second BBS locus. *Hum. Mol. Genet.*, **12**, 1651–1659.
53. Beales, P.L., Badano, J.L., Ross, A.J., Ansley, S.J., Hoskins, B.E., Kirsten, B., Mein, C.A., Froguel, P., Scambler, P.J., Lewis, R.A. *et al.* (2003) Genetic interaction of BBS1 mutations with alleles at other BBS loci can result in non-Mendelian Bardet-Biedl syndrome. *Am. J. Hum. Genet.*, **72**, 1187–1199.
54. Katsanis, N., Eichers, E.R., Ansley, S.J., Lewis, R.A., Kayserili, H., Hoskins, B.E., Scambler, P.J., Beales, P.L. and Lupski, J.R. (2002) BBS4 is a minor contributor to Bardet-Biedl syndrome and may also participate in triallelic inheritance. *Am. J. Hum. Genet.*, **71**, 22–29.
55. Ferrante, M.I., Zullo, A., Barra, A., Bimonte, S., Messaddeq, N., Studer, M., Dolle, P. and Franco, B. (2006) Oral–facial–digital type I protein is

required for primary cilia formation and left–right axis specification. *Nat. Genet.*, **38**, 112–117.
56. Marshall, W.F. and Nonaka, S. (2006) Cilia: tuning in to the cell's antenna. *Curr. Biol.*, **16**, R604–R614.
57. Otto, E.A., Loeys, B., Khanna, H., Hellemans, J., Sudbrak, R., Fan, S., Muerb, U., O'Toole, J.F., Helou, J., Attanasio, M. *et al.* (2005) Nephrocystin-5, a ciliary IQ domain protein, is mutated in Senior-Loken syndrome and interacts with RPGR and calmodulin. *Nat. Genet.*, **37**, 282–288.
58. Romio, L., Fry, A.M., Winyard, P.J., Malcolm, S., Woolf, A.S. and Feather, S.A. (2004) OFD1 is a centrosomal/basal body protein expressed during mesenchymal–epithelial transition in human nephrogenesis. *J. Am. Soc. Nephrol.*, **15**, 2556–2568.
59. Grandel, H. and Schulte-Merker, S. (1998) The development of the paired fins in the zebrafish (*Danio rerio*). *Mech. Dev.*, **79**, 99–120.
60. van Eeden, F.J., Granato, M., Schach, U., Brand, M., Furutani-Seiki, M., Haffter, P., Hammerschmidt, M., Heisenberg, C.P., Jiang, Y.J., Kane, D.A. *et al.* (1996) Genetic analysis of fin formation in the zebrafish, *Danio rerio*. *Development*, **123**, 255–262.
61. Stott, N.S. and Chuong, C.M. (1997) Dual action of Sonic hedgehog on chondrocyte hypertrophy: retrovirus mediated ectopic sonic hedgehog expression in limb bud micromass culture induces novel cartilage nodules that are positive for alkaline phosphatase and type X collagen. *J. Cell. Sci.*, **110**, 2691–2701.
62. Huangfu, D. and Anderson, K.V. (2005) Cilia and Hedgehog responsiveness in the mouse. *Proc. Natl Acad. Sci. USA*, **102**, 11325–11330.
63. Huangfu, D., Liu, A., Rakeman, A.S., Murcia, N.S., Niswander, L. and Anderson, K.V. (2003) Hedgehog signalling in the mouse requires intraflagellar transport proteins. *Nature*, **426**, 83–87.
64. Westerfield, M. (1995) *The Zebrafish Book. A Guide for the Laboratory Use of Zebrafish*, 3rd edn. University of Oregon Press, Eugene.
65. Turner, D.L. and Weintraub, H. (1994) Expression of achaete-scute homolog 3 in *Xenopus* embryos converts ectodermal cells to a neural fate. *Genes Dev.*, **8**, 1434–1447.
66. Taylor, W.R. and Dyke, G.C.V. (1985) Revised procedures for staining and clearing small fishes and other vertebrates for bone and cartilage study. *Cybium*, **9**, 107–119.